Feature article

Effect of shear flow on multi-component polymer mixtures

Charles C. Han [a,*], Yonghua Yao [a,b], Ruoyu Zhang [a,b], Erik K. Hobbie [c]

[a] *State Key Laboratory of Polymer Physics and Chemistry, Joint Laboratory of Polymer Science and Materials, Institute of Chemistry, Chinese Academy of Sciences, Beijing 100080, China*
[b] *Graduate School of Chinese Academy of Sciences, Beijing 100080, China*
[c] *Polymers Division, National Institute of Standards and Technology, Gaithersburg, MD 20899, USA*

Abstract

The effect of shear flow on the structure of multi-component polymer blends and solutions is reviewed. The techniques of small-angle light and neutron scattering, optical microscopy, and fluorescence microscopy are used to directly assess the influence of an externally applied shear field on the phase stability and morphology of model polymer blends and solutions. The polymeric fluids of interest vary from miscible blends and pseudo-binary solutions near a critical point of unmixing to thermodynamically unstable and completely immiscible blends undergoing spinodal decomposition and coarsening in the presence of simple shear flow. We review the influence that critical concentration fluctuations, viscoelasticity, and rheological asymmetry have on the shear response of polymer blends and solutions individually, and we discuss the practically important interplay of these three separate effects. We conclude our review by discussing the need for more computational and theoretical efforts focused on shear-induced structure in polymer blends.
© 2006 Elsevier Ltd. All rights reserved.

1. Introduction

There is considerable interest in the phase behavior of multi-component polymer mixtures, the so-called polymer blends, due to their broad technological importance in the plastics industry. Traditionally, quiescent conditions have been adopted for characterizing the phase behavior of polymer blends, with the majority of past work emphasizing two different but related aspects. The most prevalent is the measurement of equilibrium thermodynamic variables, such as the free energy of mixing, the composition and temperature dependent phase diagram, and the Flory–Huggins polymer–polymer interaction parameter, χ. The other most common trend has been to study the non-equilibrium kinetics of phase separation within unstable or metastable regions of the phase diagram, an area where considerable experimental and theoretical work has already been done on binary mixtures undergoing liquid–liquid phase separation through spinodal decomposition and nucleation [1–5]. Because polymer blends near a critical point of unmixing can often be adequately described by a mean-field theoretical formalism, linearized kinetic models have proven to be quite useful and relevant as a starting point for describing the growth kinetics of the unmixing process [6–11].

Although equilibrium studies of the phase behavior of polymer blends and kinetic studies of phase separation in polymeric mixtures have both greatly improved our fundamental understanding of multi-phase polymer materials, the physical properties of technologically relevant polymer blends are determined to a large extent by the morphology that develops during processing, and the commercially important area of polymer processing and engineering has not yet been able to take full advantage of this improved understanding. Thus, while shear-induced effects in polymer blends and solutions are potentially very rich and technologically important, the response of polymer blends and solutions to shear flow, a key factor in polymer processing, has only very recently been studied in a systematic manner. The ultimate goal of many manufacturing processes is to control the morphology (and hence the ultimate physical properties) of polymer blends, and typical polymer processing procedures, such as extrusion or injection molding, generally subject these soft viscoelastic multiphase materials to strong shearing flows before returning them back to a quiescent state, thus creating the essential need

for a full characterization of the influence of shear and shear history on the phase behavior of polymer blends. An exhaustive and universal description of macromolecular fluids under shear flow is clearly a challenging and somewhat daunting task. Here, we review the mechanisms by which shear flow can influence the morphology and phase behavior of polymer blends and solutions. Although theoretical models are cited and employed as needed, the review is offered from what is primarily an experimental perspective. It is hoped that the implications and conclusions will serve as a point of reference for polymer scientists and engineers working in the field of flow-induced polymer blending. It is also hoped that the paper will serve as useful starting point for further computational and experimental work directed as formulating a universal description of shear-induced structure in polymeric fluids.

Early studies of phase separation in simple binary liquids by Beysens et al. [12,13] found that shear flow can suppress critical fluctuations and lead to a true thermodynamic shift in the critical temperature, T_c. In polymer mixtures (which in the simplest approximation, due to the size of the molecules involved, exhibit mean-field behavior rather than the Ising type critical behavior characteristic of small-molecule binary mixtures), the exact nature of the experimentally observed shear induced mixing is a question that is still open to scientific debate. If a true shear-induced shift in T_c can also be observed in polymer blends of sufficiently low molecular weight, then physical insight into the unmixing process can be garnered by following the evolution from quiescent thermodynamic equilibrium to a non-equilibrium state that is distorted by the shear field. This information might then be used as a foundation for a description of flow induced mixing in the more technologically relevant scenario in which the components are high relative molecular mass polymers with intrinsic viscoelasticity.

Since the earliest descriptions of shear-induced phase transitions in polymer solutions [14], both mixing and demixing (phase separation) have been observed in response to an applied external shear stress [14–21]. These phenomena have been interpreted as a shift in the coexistence curve and a distortion of concentration fluctuations induced by the shear field. Some studies have found the common feature that sheared semidilute polymer solutions near the coexistence curve exhibit a 'butterfly' light scattering pattern associated with an anisotropic enhancement of concentration fluctuations [19,22–24] and theoretical treatments have been developed to explain these results [25,26]. Rangel-Nafaile et al. [27] and Tirrel [28] discuss flow-induced turbidity in polymer fluids at temperatures beyond the equilibrium coexistence curve of the quiescent solution. Such previous work suggests that shear flow causes apparent shifts in the phase boundaries [29,30] of various two component polymer blends, denoted as either flow-induced mixing (FIM) [30–32] or flow-induced demixing (FID) [33–35]. These observations have spawned calculations for FID in lattice-Boltzmann fluid mixtures [36]. For an extensive review of previous experimental work, reviews written by Larson [37] and Tirrel [28], which cover FIM and FID, stress-induced diffusion, shear-induced polymer

migration, and the effects of flow on crystalline, liquid-crystalline, and block-copolymer ordering transitions, are particularly useful. Although the effect of adding copolymer as interfacial modifier is an important practical area of polymer blending and the different behaviors observed under shear are quite intriguing [38–44], here we focus specifically on miscible and immiscible polymer blends under simple steady shear flow.

A number of experimental methods have been developed to probe the influence of shear flow on complex fluids, including light scattering [45], small angle neutron scattering [46], small angle X-ray scattering [47], optical rheometry [48] and flow birefringence [49]. Recent developments in methods and instrumentation are reviewed by Nakatani [50]. When choosing an appropriate experimental approach, attention must be paid to the length scale of interest and the specific contrast mechanism to be exploited. The type of instrumentation chosen, as well as the thermal and mechanical history of the viscoelastic polymer samples, will play a key role in dictating the design, conduct, and interpretation of experiments.

In Section 2 of this paper, a short review of the basic aspects of the equilibrium and non-equilibrium phase behavior of quiescent polymer blends is given, including relevant underlying theories and a brief review of experimental data. After discussing the unperturbed phase behavior, the response of these systems to simple steady shear flow is described in Sections 3 and 4. Shear-induced phase behavior in the one and two-phase regions are compared. Experimental results have been obtained on a variety of different polymer blend systems using a variety of methods. Small-angle neutron scattering (SANS), light scattering (LS), and phase-contrast optical microscopy (PCOM) are utilized to probe the dynamics of FIM and FID and the kinetics after a 'shear quench' into the two-phase region of the phase diagram. We also specifically introduce fluorescence microscopy (FM) as a tool for measuring the composition difference, $\Delta\phi$, in phase separating polymer blends under shear. The effect of shear flow on concentration fluctuations in the miscible phase will be compared with measurements of the steady-state morphology in the two-phase region to map out generic non-equilibrium trends as a function of quench depth, shear rate, and the rheology of the pure melt components.

2. The quiescent state—fluctuations and spinodal decomposition

Here we give a brief overview of fluctuations and spinodal decomposition in quiescent polymer blends [51–55]. We use the temperature dependence of the inflection point $(\partial\Delta f/\partial\Phi)_{T,P}=0$, where Δf is the free energy of mixing, to define the binodal curve, and $(\partial^2\Delta f/\partial\Phi^2)_{T,P}=0$ to define the spinodal curve. In the one-phase or miscible region of the phase diagram, concentration fluctuations are stable, but they become slower and larger in scale as the spinodal curve is approached. When a binary mixture is suddenly brought from a point in the miscible region of the phase diagram to a point within the spinodal region of the phase diagram, where $(\partial^2\Delta f/\partial\Phi^2)<0$,

spontaneous phase separation occurs though the growth of unstable concentration fluctuations. A description of fluctuations within the one-phase region is given by the classic theory of de Gennes. A description of spinodal decomposition in the two-phase region is divided into three stages; early, intermediate, and late. Based on current understanding, the linearized theory of Cahn, Hilliard and Cook [6–11] (CHC) provides us with a rather simple and usually sufficient description of the earliest stages of spinodal decomposition in binary macromolecular fluids. Modified theories that include a degree of non-linearity have been used to analyze data for the intermediate stage, while scaling arguments have generally been utilized to interpret the phase separation kinetics in terms of hydrodynamics and domain coarsening in the later stages [5].

Within the one-phase or stable region of the phase diagram, the random phase approximation (RPA) for the static structure factor of polymer mixtures is a mean-field, self-consistent theory originally developed by de Gennes [56]. It gives the static structure factor for a miscible binary mixture of polymers A and B as

$$S(q) = k_n\{[\phi_A N_A v_A f(u_A)]^{-1} + [\phi_B N_B v_B f(u_B)]^{-1} - 2\chi/v_0\}^{-1},$$

(1)

where

$$k_n = N_0(a_A/v_A - a_B/v_B)^2,$$

(2)

with N_0 being Avogadro's number, v_0 and v_i the molar volumes of a reference unit cell and of the i-th monomer, respectively, and a_i the scattering length per mole of the i-th component. The single-chain structure factor, $f(u_i)$, is given by the Debye function

$$f(u_i) = (2/u_i^2)[\exp(-u_i) - 1 + u_i]$$

(3)

where $u_i = q^2 R_{gi}^2$, $q \equiv |\mathbf{q}| = (4\pi/\lambda)\sin(\theta/2)$ is the magnitude of the scattering wave vector (λ is the incident beam wavelength and θ the scattering angle), and R_{gi} is the radius of gyration of the i-th component. In the limit of small q, Eq. (1) reduces to the Lorentzian form, $S(q) = S(0)(1 + \xi^2 q^2)^{-1}$, in terms of the susceptibility, $S(0)$, and correlation length, ξ. Both of these quantities diverge at the critical point, reflecting the appearance of long-lived, long-wavelength fluctuations in composition. Within the mean-field RPA formalism, the critical exponents characterizing this divergence are $\gamma = 1$ and $\nu = 1/2$ for $S(0)$ and ξ, respectively. Sufficiently close to the critical point, critical fluctuations typically become important and these exponents crossover to values more characteristic of the three-dimensional Ising universality class; approximately $\gamma = 1.24$ and $\nu = 0.63$ for $S(0)$ and ξ, respectively [1]. It is the presence of these large slow composition fluctuations that makes the response of these fluid mixtures to shear flow so intriguing. The assumption of incompressibility used in the original derivation has been reconsidered by Sanchez [57], Hammouda and Benmouna [58], and Taylor et al. [59].

In the spinodal region of the phase diagram, the long wavelength concentration fluctuations described above become unstable and start to grow via spinodal decomposition. In the area bounded by the spinodal and the binodal, these fluctuations are metastable and phase separation proceeds via nucleation. According to a modified CHC theory extended to polymers [51–55], the time dependent structure factor, $S(q,t)$, can be well described by the CHC formalism in the early stage
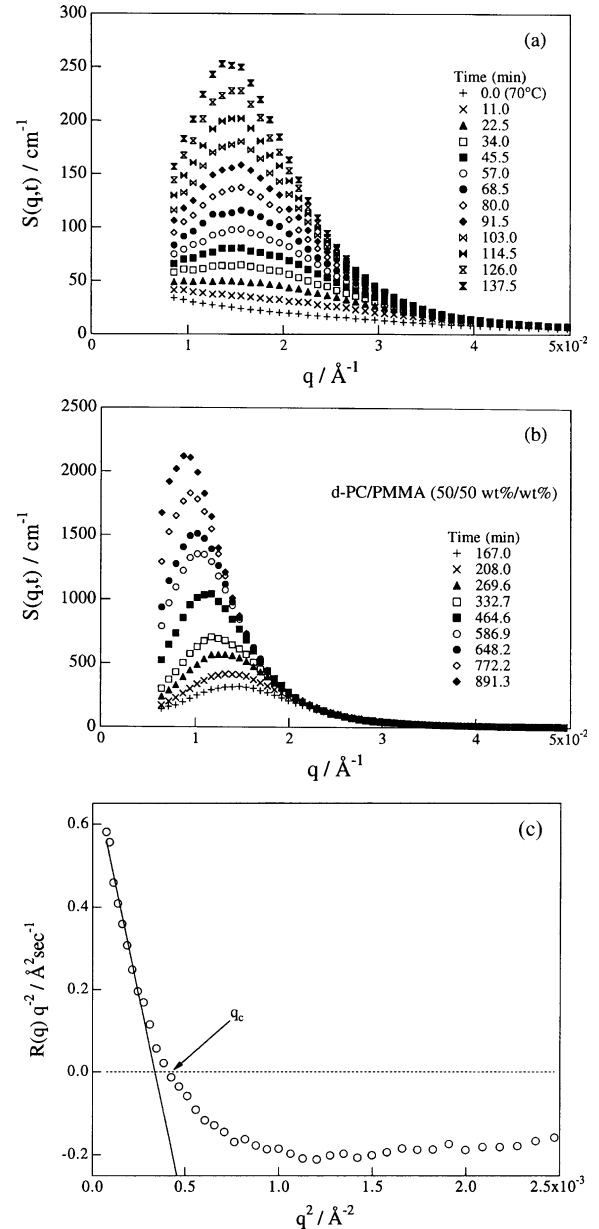
Fig. 1. (a) The time-dependent structure factor for a dPC/PMMA (50:50 by mass) blend in the early stage of spinodal decomposition measured by SANS, with intensity growth at constant q_{max}. The growth rate of concentration fluctuations follows from the peak intensity. (b) The time-dependent SANS structure factor for the same blend in the late stage of spinodal decomposition, where the intensity is higher than in the early stage. (c) A plot of $R(q)/q^2$ versus q^2 shows a limiting linear region at small q, where the interdiffusion coefficient can be extrapolated and the virtual structure factor obtained. It is unique to polymer systems that at q values greater than q_c, $R(q)$ becomes negative and deviates from a straight line. This implies that the segmental motion within a single chain is still (diffusive) relaxation, despite the polymer center of mass undergoing phase separation. Data were first presented in Ref. [63].

of spinodal decomposition, which is characterized by the growth of fluctuations of a fixed length scale, $2\pi/q_c$, and the associated appearance of a well defined but stationary spinodal peak in $S(q,t)$, as shown in Fig. 1(a). When the spinodal peak starts to move, as shown in Fig. 1(b), the linearized CHC theory becomes inadequate. In the linear regime, the composition profile starts to evolve toward thermal equilibrium but the structure does not coarsen. Within the linear CHC formalism, the non-equilibrium structure factor is

$$S(q,t) = S_\infty + [S_0(q) - S_\infty(q)]\exp[2R(q)t] \qquad (4)$$

where $S_\infty(q)$ is the virtual structure factor,

$$S_\infty(q) = k_B T/[(\partial^2 \Delta f/\partial \phi^2)_0 + 2\kappa q^2] \qquad (5)$$

The growth rate is

$$R(q) = -Mq^2[(\partial^2 \Delta f/\partial \phi^2)_0 + 2\kappa q^2] = -D_{int}q^2 - 2M\kappa q^4, \qquad (6)$$

with $q_c^2 = -(\partial^2 \Delta f/\partial \phi^2)_0/2\kappa$. The interdiffusion coefficient, $D_{int} = M(\partial^2 \Delta f/\partial \phi^2)_0$ where M is the mobility, can be extrapolated from the linear regime of $R(q)/q^2$ versus q^2, as shown in Fig. 1(c).

After the earliest stage, the amplitude of concentration fluctuations and the characteristic length scale of these fluctuations both increase with time. The spinodal peak in $S(q,t)$ becomes sharp and its position, $q_{max}(t)$, starts to gradually decrease as the structure grows in scale, as shown in Fig. 1(b). In this stage, scaling arguments can be used to analyze experimental results by plotting a reduced characteristic length scale as a function of a reduced time [60,61]. Akcasu et al. have extended the calculation of $S(q,t)$ for binary liquids to polymer mixtures and derived an analytical expression appropriate to the intermediate stages of SD [51].

Unlike the middle stage, the most important characteristic feature of the late stage of SD is a disruption of the co-continuous structure, which starts to coarsen with time in a self-similar way through hydrodynamic processes, following mechanisms first suggested by Siggia [62]. At this stage, the composition of the microdomains has reached the equilibrium coexistence values, ϕ_A and ϕ_B, while the interface has developed an equilibrium profile. The spinodal peak intensity and position typically change with time in a self-similar power law fashion that can often again be scaled in terms of dimensionless length and time, with $S(q,t) = q^{-d}f(q/q_{max})$, where d is the dimension characteristic of the morphology.

The literature contains many examples of experimental and theoretical studies of the kinetics of phase separation in polymer fluids. To study early stage spinodal decomposition in polymer blends using SANS, for example, measurements of $S(q,t)$ for phase separating polycarbonate ($M_w = 2.81 \times 10^4$) and poly(methyl methacrylate) ($M_w = 3.30 \times 10^4$) blends near the glass transition temperature have been performed [63], as shown in Fig. 1. In that situation, shallow quenches are not required to keep q_{max}, the wavevector corresponding to the fastest growing fluctuation mode, in the experimental q range. The glass transition is exploited to prepare the system in a 'frozen' miscible state before bringing the specimen to

a temperature slightly above the glass transition for time-resolved SANS measurements of $S(q,t)$. As in other work [40,64,65], the linearized solution of the mean-field CHC formulation provides a sufficient description of the data. Dudowicz and Freed have conducted a detailed analysis of
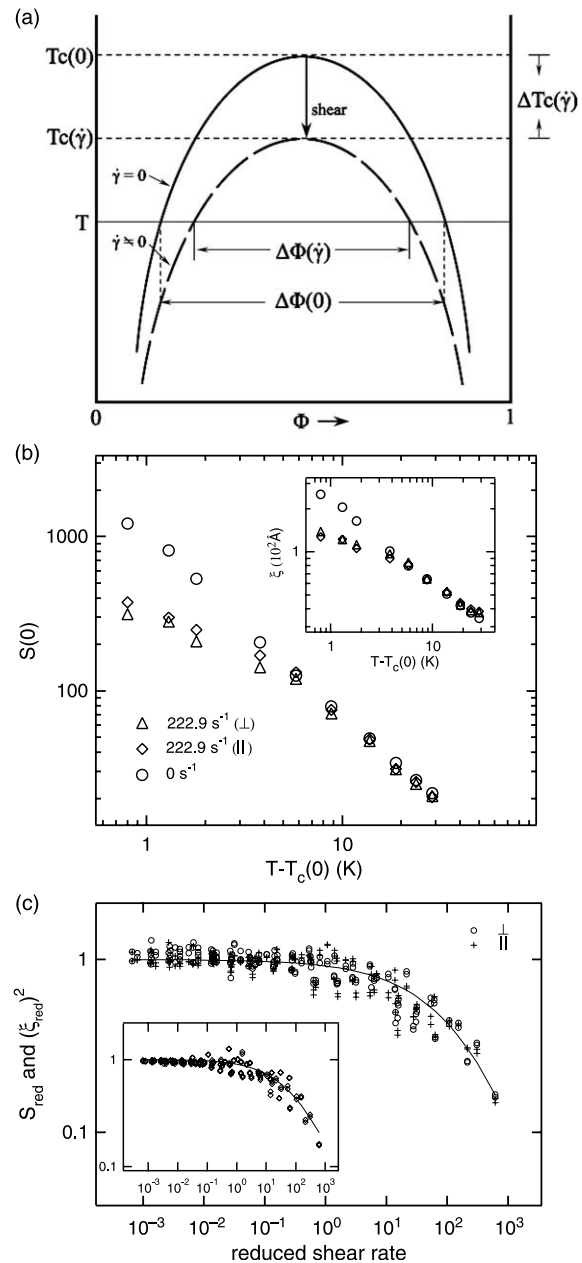
Fig. 2. (a) Schematic representation of the mixing effect of shear flow on the phase boundary of a low relative molecular mass polymer blend. (b) The shear-induced shift in the critical temperature of a low-molecular weight PSD-PB blend is apparent in the temperature and shear rate dependence of the non-equilibrium susceptibility and thermal correlation length (inset). (c) The relative shifts of the type shown in (b) collapse onto a universal scaling curve that can be directly compared with the theoretical prediction for the shear-induced shift in T_c, shown as a solid curve in both plots. Data in the main panel are sector averaged along the flow (||) and vorticity ($\perp$) directions, while those in the inset are circularly averaged. There are no free parameters in this comparison with theory, which we originally reported in Ref. [74].

such results and obtained good agreement between theory and experiment [66–68].

3. Effect of shear on composition fluctuations—phase separation and inversion

3.1. The one phase region

The mode-coupling renormalization-group (MCRG) theory of a simple binary fluid has been used to model the critical dynamics and shear response of polymer mixtures and solutions. This is model H in the classification scheme of Hohenberg and Halperin [1] with a convective time derivative appropriate to the geometry of shearing. From the Onuki–Kawasaki MCRG analysis [21,69–71], the shear rate dependence of the critical temperature can be expressed as

$$[T_c(\dot{\gamma}) - T_c(0)]/T_c(0) \approx -r[0.0832\varepsilon + \mathbf{O}(\varepsilon^2)](\dot{\gamma}\tau_c)^{1/3v} \quad (7)$$

where $T_c(0)$ is the equilibrium critical temperature, $r = 1 - T_c(0)/T$ is the equilibrium reduced temperature, $\varepsilon = 4 - d$ is an expansion parameter (where $d = 3$ is the spatial dimension), and $\tau_c = \xi^2/D_c$ is the characteristic lifetime of the equilibrium concentration fluctuations, where D_c is the critical diffusion coefficient. The exponent $v = 0.63$ in Eq. (7) is the critical correlation length exponent appropriate to the three-dimensional Ising universality class. This equation relates the change in critical temperature to the break-up of large scale critical fluctuations by the flow, as represented schematically in Fig. 2(a).

To test this prediction, a deuterated polystyrene/polybutadiene (PSD/PB) blend was studied by combining quiescent dynamic light scattering (DLS) and SANS with SANS under shear flow [72–74]. The polymer components used were low molecular mass ($M_{wPSD} = 9 \times 10^2$, $M_{wPB} = 5 \times 10^3$) to ensure a significant temperature window of critical fluctuations [75]. The phase diagram exhibits upper critical solution temperature (UCST) behavior with a critical composition of 72% by mass PSD and a critical temperature of 41.2 °C. From measurements of the equilibrium critical dynamics, the equilibrium lifetime of critical fluctuations, $\tau_c = \xi^2/D_c$, can be used to distinguish the 'weak shear' limit ($\tau_c\dot{\gamma} \ll 1$) from the 'strong shear' limit ($\tau_c\dot{\gamma} \gg 1$). When the shear rate becomes comparable to the equilibrium relaxation rate of these fluctuations, τ_c^{-1}, long-range critical fluctuations begin to break apart. Although the original MCRG calculation is quite involved, the physics can be explained very intuitively. By fitting the non-equilibrium SANS structure factor, $S(\mathbf{q}, \dot{\gamma})$, to the Lorentzian form obtained from the Onuki–Kawasaki theory [74] at length scales relevant to SANS, the non-equilibrium susceptibility, $S(0, \dot{\gamma})$, and correlation length, $\xi(\dot{\gamma})$, can be extracted, with the asymptotic expressions

$$S(0, \dot{\gamma}) \propto [1 - T_c(\dot{\gamma})/T]^{-\gamma} = S(0)(1 + \Delta r/r)^{-\gamma} \quad (8)$$

and

$$\xi(\dot{\gamma}) \propto [1 - T_c(\dot{\gamma})/T]^{-v} = \xi(1 + \Delta r/r)^{-v}, \quad (9)$$

where $\gamma \approx 2v$ and $\Delta r/r = [0.0832\varepsilon + \mathbf{O}(\varepsilon^2)](\dot{\gamma}\tau_c)^{1/3v}$. Fig. 2(b) shows how $S(0, \dot{\gamma})$ and $\xi(\dot{\gamma})$ are suppressed by shear in the vicinity of the quiescent critical point, reflecting the true shear-induced shift in T_c.

The reduced susceptibility, $S_{red} = S(0, \dot{\gamma})/S(0)$, and the reduced correlation length, $\xi_{red} = \xi(\dot{\gamma})/\xi$, can then be expressed in terms of the reduced shear rate, $\tilde{\gamma} = \dot{\gamma}\tau_c$, as

$$S_{red} = \xi_{red}^2 \approx \{1 + [0.0832\varepsilon + \mathbf{O}(\varepsilon^2)]\tilde{\gamma}^{1/3v}\}^{-2v} \quad (10)$$

If the flow has no effect, then S_{red} and ξ_{red} are both 1, as in quiescence. When the flow starts to suppress long-wavelength critical fluctuations, S_{red} and ξ_{red} begin to decrease, reflecting a decrease in the low-q scattering intensity. In this way, the quantities S_{red} and ξ_{red} are direct measures of the influence of shear flow on critical fluctuations. Fig. 2(c) shows reduced susceptibility and reduced correlation length squared plotted as
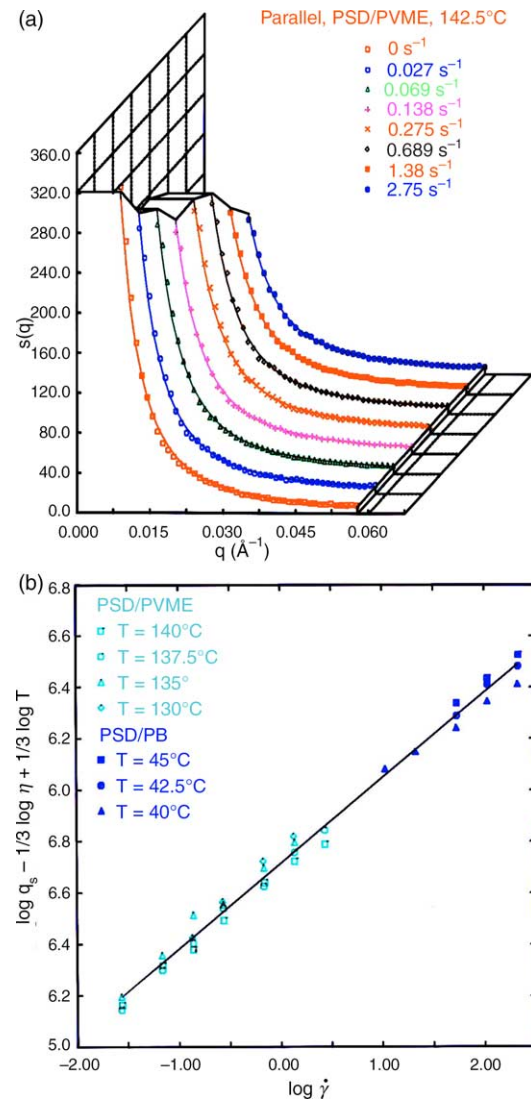
Fig. 3. (a) The suppression of the scattering structure factor parallel the flow direction showing the shear distortion of concentration fluctuation near the critical point. (b) The experimentally determined crossover wavenumber, q_s, as a function of temperature and shear rate gives the inverse size scale of the lowest wavelength fluctuation mode which is not affected by shear. These results were originally published in Ref. [30].

a function of reduced shear rate for all of the shear rates and temperatures used in the study. The fitted universal scaling curve contains no free parameters and corresponds to the right-hand side of Eq. (10) to $\mathbf{O}(\varepsilon)$ for $d=3$. The agreement with theory is excellent over six decades in reduced shear rate. As noted above, the intuitive explanation is that flow starts to break apart long-wavelength critical fluctuations when the shear rate becomes comparable to the equilibrium relaxation rate of these fluctuations. This is evidenced by the fact that both S_{red} and ξ^2_{red} begin to deviate from unity at $\tilde{\gamma} \approx 1$. Since any component with an equilibrium lifetime greater than τ_c will essentially be suppressed by the flow, it is natural that the size of critical fluctuations is limited by shear when $\dot{\gamma} \geq \tau_c^{-1}$. The same physical scenario was also verified in an analogous manner for a pseudo binary mixture of higher molecular weight DPS and PB in a common good solvent, where the effect of dilution is to enhance the temperature window where critical fluctuations become important (with respect to a blend of the pure melt components) [76]. The width of this temperature window decreases rapidly as the bare correlation length increases, in accordance with the well known Ginzburg criterion [72]. In this regard, dilution of high molecular weight components has the same effect as lowering molecular weight because it decreases the free energy cost of a concentration gradient.

Another comparative experiment[30] was done to study the shear rate dependence of entangled versus unentangled chains, LCST versus UCST behavior, and critical versus off-critical compositions by using PSD/PVME and the same PSD/PB blend described above. The PSD/PVME blend consisted of high molecular mass polymers ($M_{w\ PSD}=2.7\times10^5$, $M_{w\ PVME}=1.8\times10^5$) and exhibited lower critical solution temperature (LCST) behavior at a critical composition of 80/20 mass ratio PSD/PVME. In this study, a slightly off-critical composition of the UCST PSD/PB blend was used (50/50 mass ratio of PSD/PB). The q dependence of $S(\mathbf{q},\dot{\gamma})$ projected along the direction of flow is shown in Fig. 3(a). There is a suppression of fluctuations along the flow direction, but no apparent effect along the direction of vorticity. In comparison, the PSD/PB blend shows the same isotropic suppression of fluctuations described in detail in the preceding paragraphs. We can define the largest mode unaffected by shear as q_s^{-1}, where q_s denotes the characteristic wavevector at which the structure factor first deviates from its quiescent shape. From a simple rotary diffusion model, all of the crossover modes for these two seemingly different polymer blend systems are found to scale according to

$$q_s = (8\pi\eta/k_BT)^{1/3}\dot{\gamma}^{1/3}, \tag{11}$$

as shown in Fig. 3(b). We note that the dynamic mode-coupling analysis of Kawasaki [4] gives a somewhat similar prediction for the crossover wave vector,

$$q_{c\dot{\gamma}} = (16\eta/k_BT)^{1/3}\dot{\gamma}^{1/3}, \tag{12}$$

and we suggest that this seemingly universal behavior arises from the ubiquitous importance of hydrodynamic coupling in

the critical dynamics of polymer blends, independent of the importance of static critical fluctuations [77,78]. To see this, one need simply equate the characteristic timescale for the thermal diffusion of a composition fluctuation of size $2\pi/q_s$ in a fluid of viscosity η with the timescale externally imposed by the shear field.

3.2. Two phase region

If the shearing experiment is started at a temperature below the quiescent critical point, it is interesting to ask—particularly in light of the above observations of shear-induced mixing—how the phase separation process is altered by the flow. Because of the large scale morphology associated with intermediate and late stage phase-separation in polymer blends, a number of different research groups have probed various aspects of multi-component polymer systems under shear using light scattering and optical microscopy. Hashimoto and co-workers [29,79–82] have done extensive work, and similar results have been found by other research groups. For a pseudo binary polymer/polymer/solvent mixture in the two-phase region (e.g. blends of polystyrene (PS) and polybutadiene (PB) dissolved in dioctyl phthalate (DOP)), there are five distinct behavior types under steady shear flow. The first regime (regime I) is defined by quiescent conditions where the sample is fully phase separated into macroscopic polystyrene-rich and polybutadiene-rich layers. An incident laser beam normal to these layers produces very little scattered light intensity. In the next regime (regime II, defined by very weak shear) the layers break up into droplets or a highly interconnected structure, which displays very little anisotropy. The light scattering patterns observed in this regime are also fairly isotropic. In regime III, the droplets become elongated along the flow direction and the scattering intensity is diminished in the direction parallel to the flow, while the intensity remains constant or increases slightly in the direction perpendicular to the flow. In regime IV, the scattering intensity perpendicular to flow also starts to diminish and the scattering anisotropy becomes highly pronounced. This regime has been interpreted as the onset of remixing, where the concentration difference between the two phases starts to decrease. The highly elongated droplets observed in regime III and IV have been referred to as a 'string phase'. Finally, in regime V, the only scattering is low-intensity critical scattering, and the sample is presumed to be thermodynamically remixed on optical length scales.

Similar studies by our group have focused on not only the ternary PS/PB/DOP system, but also on undiluted blends of PS/PB [31]. To make our observations more quantitative and to emphasize some of the important underlying physics, we have used an effective single droplet model motivated by the classical work of Taylor on isolated droplets in definable fields of flow [83]. The work of Taylor demonstrates that an initially spherical droplet under shear in a fluid of the same viscosity deforms into an ellipsoid of major axis $R_{\parallel}$ and minor axis $R_{\perp}$ with aspect ratio $\zeta=R_{\parallel}/R_{\perp}$. The Taylor result for a single

droplet can be recast as

$$\zeta = R_{\parallel}/R_{\perp} = (1 + \tau_c\dot{\gamma})/(1 - \tau_c\dot{\gamma}) + ... \qquad (13)$$

where the characteristic droplet relaxation time $\tau_c = \eta R_0/\sigma$ is given in terms of the viscosity, η, the unperturbed radius, R_0, and the interfacial tension, σ. In an idealized scenario with equal viscosities inside and outside the droplet, the deformed drop breaks apart when the shear rate reaches a threshold value $\dot{\gamma}_c \propto \sigma/2\eta R_0$, or when the shear stress becomes comparable to the capillary pressure [83]. The factor of two reflects the empirical dependence of critical capillary number on the stated parameters, which says that a droplet in a fluid of comparable viscosity breaks at a critical capillary number of 2–3. Since $\dot{\gamma}_c$ depends on R_0, large droplets breaks at lower shear rates, which explains why droplet size distributions have been observed to become more monodisperse with increased shearing. Note that the reduced shear rate $\tilde{\gamma} = \dot{\gamma}\tau_c$ in Eq. (13) is analogous to the Capillary number of an isolated droplet. Although the construct of an effective single droplet model for what is in reality a polydisperse suspension of soft interacting droplets is somewhat over-simplified, anyone who has computationally studied the deformation and rupture of an isolated viscous droplet in shear will appreciate the inherent challenges and the subsequent need for some type of intuitive and transparent foundation. The most obvious over simplification is the deviation of the flow profile from a simple linear shape due to the presence of many interacting soft domains. Onuki has made a more rigorous extension of the Taylor model to a thermodynamically unstable binary fluid [71,84–86]. Droplets of the minority phase reach a steady state at low shear rate, and then start to elongate and break repeatedly with increasing shear as in the Taylor picture. In the strong-shear limit, the droplets become highly elongated, giving way to a string-like structure factor.

A simple combination of classical hydrodynamics and MCRG theory has been used to quantify the crossover from droplets to strings [87]. The key element of such an interpretation is that the surface tension in a critical fluid is [88] $\sigma \approx 0.1k_BT/\xi^2$, where ξ is the thermal correlation length defined in Section 2. Under weak shear, the flow is assumed to merely stabilize the phase separation process. As the mixture moves toward the phase boundary in response strong shear, the interfacial tension softens with increasing shear rate, until eventually the one-phase state is restored. From this perspective, it is easy to understand why these string-like patterns form, since from a purely hydrodynamic perspective they would not be anticipated for droplets of comparable viscosity and finite interfacial tension. Close to the critical point but just inside the two-phase regime, there is little distinction between droplet and matrix and the domains simply deform along streamlines into 'strings'. As an example, we consider polystyrene ($M_w = 96 \times 10^3$) and polybutadiene ($M_w = 22 \times 10^3$) with DOP as a common good solvent [89]. The critical temperature of the mixture is 68 °C at a critical composition of 30/70 PS/PB by mass, with a total of 8% polymer by mass in DOP. Online optical microscopy and light scattering data [116] for the breakup sequence at an off-critical
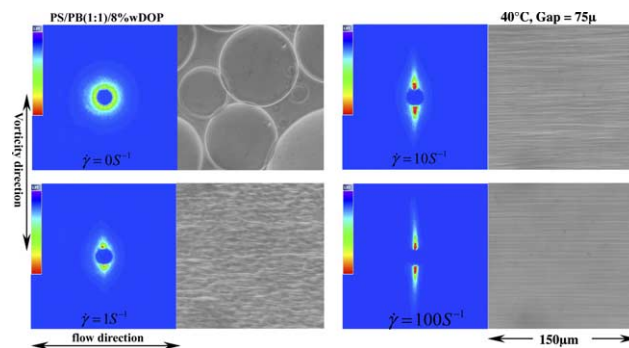
Fig. 4. Light scattering/micrograph pair as a function of shear rate for an off-critical PS/PB/DOP system (50/50 mass ratio of PS/PB, total 8 mass% concentration of the polymer in DOP) undergoing phase separation.

composition quenched well into the two-phase regime is shown in Fig. 4. Spherical droplets elongate and break repeatedly until the domain pattern becomes string-like.

The shear rate dependence of the mean aspect ratio during break up and elongation can be tabulated as shown in Fig. 5. Data for both the PS/PB/DOP system and a low-molecular weight PS/PB blend are compared and found to scale at different temperatures and shear rates. The polystyrene/polybutadiene blend [31] consisted of low molecular mass polymers ($M_{w\,PS} = 3 \times 10^3$ and $M_{w\,PB} = 3 \times 10^3$) with a critical composition of 60% PS by mass and a critical temperature of 134.2 °C. The reduced shear rate is as defined for Eq. (13) and the semi-quantitative computation scheme of Hobbie et al. is described in Ref. [87]. In this case, the time scale τ_c used to reduce the shear rate is directly measured by fitting ensemble averages of droplet aspect ratio to Eq. (13) in the limit of low $\dot{\gamma}$ for each mixture at each temperature and composition [31], so that τ_c can be viewed as the characteristic timescale for droplet
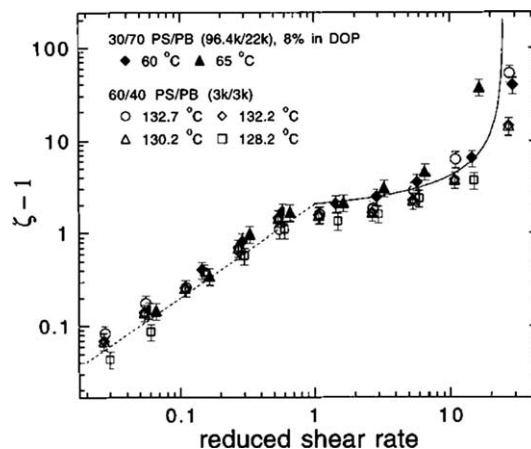
Fig. 5. Double logarithmic plot of the aspect ratio evolution as a function of reduced shear rate for a variety of polymer mixtures in the vicinity of a critical point. The dashed line represents the weak-shear (Taylor) limit, while the solid curve represents the crossover to the strong-shear limit where thermodynamic mixing starts to influence the response through a reduction in the interfacial tension. The two limits are separated by reduced shear rate of unity, which can resemble a Deborah number for a multi-phase system with interfacial viscoelasticity. In an effective single droplet picture, however, the horizontal axis is more appropriately defined as an effective Capillary number. Data were originally published in Ref. [31].

deformation in weak shear. Again, the data clearly show two distinct regimes that delineate weak and strong shear flow. In the weak shear regime, the response is of the Taylor type, with modest deformation. In the strong shear regime, the droplets start to rupture and the two components start to mix thermodynamically. As the interfacial tension vanishes, the aspect ratio becomes quite large.

Central to all of the phenomena reviewed up to this point is the idea that shear flow causes a true shift in the phase boundary or critical temperature. Given its importance, this effect has been studied directly by using fluorescence microscopy to track the composition of a two-phase polymer blend undergoing spinodal decomposition under steady shear flow [90]. NBD-labeled polystyrene ($M_w = 110 \times 10^3$) and unlabeled polybutadiene ($M_w = 22 \times 10^3$) were used with DOP as a common good solvent, where 4-chloro-7-nitrobenzofurazan (NBD chloride) was added as a fluorophore to label the polystyrene (PS). With 8% total polymer by mass in DOP, the mixture exhibits UCST behavior with a critical temperature of 86.5 °C at a close-to-critical composition of 30/70 PS/PB. Because of the tendency for the dye to quench at high temperatures, the experiment is restricted to the equilibrium two-phase region below the quiescent critical temperature, $T_c(0)$. Fig. 6(a) and (b) shows simultaneous fluorescence and phase-contrast images of PS-rich droplets coarsening in a PB-rich matrix in the late stages of spinodal decomposition.

When the reduced shear rate, $\tilde{\gamma} = \dot{\gamma}\tau_c$, is again introduced (as in Fig. 5), the data are once again found to collapse onto a universal scaling curve, as shown in Fig. 6(c). Although the droplets become small and fluorescence intensity changes become difficult to measure, the data in Fig. 6(c) show a clear tendency for $\Delta T_c(\dot{\gamma})$ to saturate at extremely high shear rates. As in Fig. 5, the characteristic timescale τ_c used to reduce $\dot{\gamma}$ in Fig. 6(c) is directly measured by fitting ensemble averages of droplet aspect ratio at each shear rate to Eq. (13) in the limit of weak shear at each temperature. The curve in Fig. 6(c) is the empirical expression

$$\frac{\Delta T_c(\tilde{\gamma})}{\Delta T_c(\tilde{\gamma} \to \infty)} = \frac{0.2\tilde{\gamma}^{0.44}}{1 + 0.2\tilde{\gamma}^{0.44}}, \quad (14)$$

which approaches unity at high shear rates. Such a 'mixing plateau' is inconsistent with the leading-order MCRG prediction, but the power-law behavior in the limit of small $\tilde{\gamma}$ can be compared with the MCRG prediction of $\tilde{\gamma}^{0.53}$. A clue into the origin of the mixing plateau might lie in the observation that it coincides with the emergence of the 'butterfly' light-scattering pattern, which is typically associated with shear-induced turbidity in semi-dilute polymer solutions [31], pointing toward the importance of viscoelastic effects that up to now have been ignored.

Indeed, the assumption of equal viscosities used in all the examples cited above is unrealistic from the practical viewpoint of processing real polymer blends, which can often exhibit disparities in the viscoelastic properties of the constituent macromolecular components. Analogous droplet-to-string progression associated with shear-induced mixing is
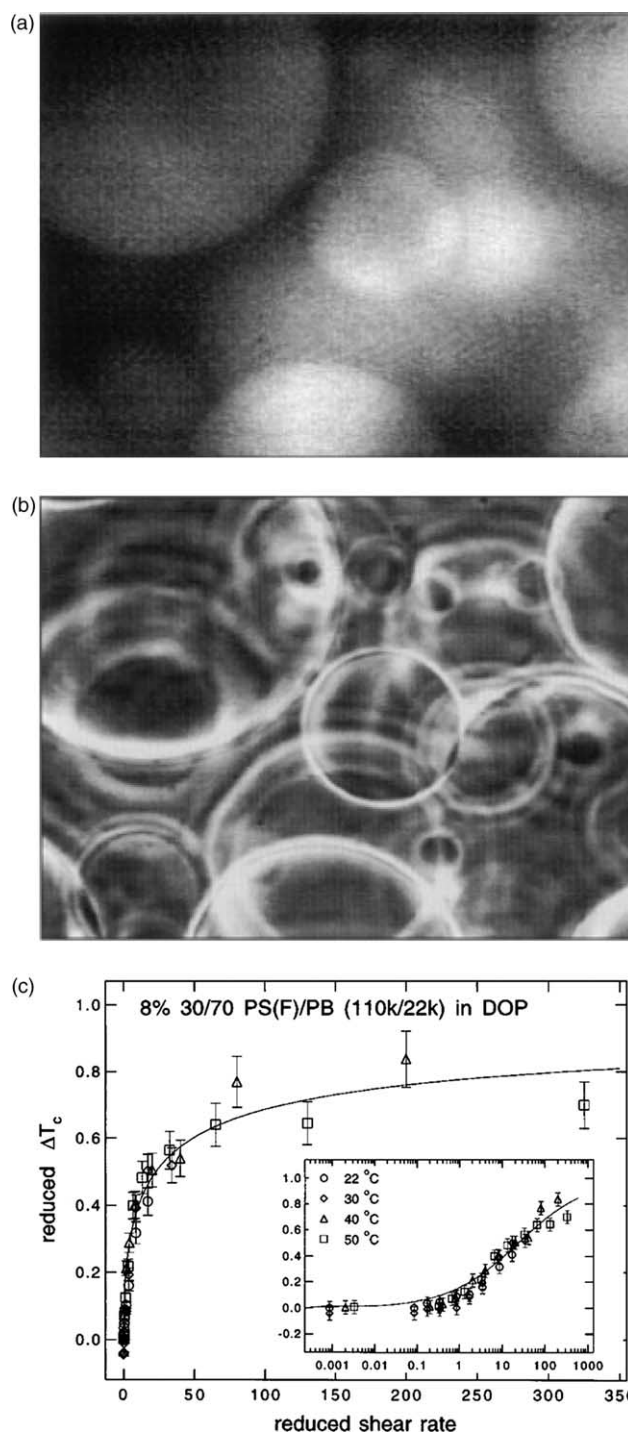
Fig. 6. Comparison between fluorescence (a) and phase contrast (b) microscopy images of PS-rich droplets coarsening in the unstable regime of the pseudo-binary mixture NBD-PS/PB/DOP at 22 °C. From images of the type shown in (a) and (b), the shear-induced shift in T_c can be deduced as a function of shear rate and temperature, which is shown in the lower panel on a reduced dimensionless scale as a function of the reduced shear rate used in Fig. 5. The inset shows a linear-log plot of the same data, where mixing begins when the reduced shear rate becomes comparable to unity. These results were originally published in Refs. [31,90].

found in critical and off-critical blends of low-vinyl polybutadiene and low-vinyl polyisoprene (LPB/LPI) [91,92], but in this case the viscosities of the neat melt components differ by a factor of three and an extension of the MCRG theory to such a more realistic scenario has not yet been made. Recent simulation work that attempts to account for this difference in shear viscosity shows agreement with experiment on one side of the critical composition but not on the other [93]. Experimentally, such blends still exhibit a true shift in the phase boundary under shear, and the homogenizing effect of the flow plays the same central role in the onset of string formation [92].

3.3. Immiscible blends

By comparison, completely immiscible blends of low-vinyl polybutadiene ($M_{LPB} = 5.1 \times 10^4$) and high-vinyl polyisoprene ($M_{HPI} = 7.2 \times 10^4$) with order-of-magnitude asymmetry in the viscoelasticity of the pure melt components represent an entirely different and perhaps more practically relevant class of polymer blends [91]. True thermodynamic mixing is absent in these multiphase mixtures, with the domain morphology being dictated entirely by hydrodynamics, the rheology of the pure polymer melt components, and droplet-droplet interactions [94]. When the more viscoelastic melt is the droplet phase, initially spherical emulsions break up into irregular looking domain patterns that show the characteristic butterfly light scattering pattern at high shear rates. Again, the single droplet response provides a useful if somewhat oversimplified point of reference, and in this case the inherent instability of a viscoelastic droplet in a less viscous matrix under simple steady shear flow is key [95]. The domain structure that develops at a shear rate of 75 s^{-1} for a 20% HPI by mass HPI/LPB blend is shown in the upper left panel of Fig. 7(a). Thresholding this image yields a map of the HPI domains, as shown in the upper right panel of Fig. 7(a), from which the orientation of long wavelength fluctuations in structure can be extracted (lower left and right panels, Fig. 7(a)). Note that the mean orientation of domains is along the vorticity direction, reflecting the mean shear-induced orientation of an individual viscoelastic droplet under comparable flow conditions [95].

The light scattering pattern associated with this structure is shown in Fig. 7(b), with a cartoon that depicts a nearly random distribution of tilted domains with mean orientation along the vorticity axis. To understand the shape of the structure observed in reciprocal (q) space, we compute the two-point composition correlation function $c(r)$ from ensembles of binary images of the type shown in Fig. 7(a). As shown in the upper left panel of Fig. 7(c), $c(r)$ has the same wing-like structure as the LS pattern, and its FFT (upper right panel, Fig. 7(c)) reproduces the butterfly

The upper right panel shows the Fourier transform of $c(r)$, which closely resembles the light-scattering pattern, $S(q)$, in (b). The main panel shows projections of $c(r)$ and $S(q)$ (inset) along the flow and vorticity directions. Weak minima along the flow direction in $c(r)$ gives rise to the winglike structure of $S(q)$ in (b). Data were originally presented in Ref. [94].
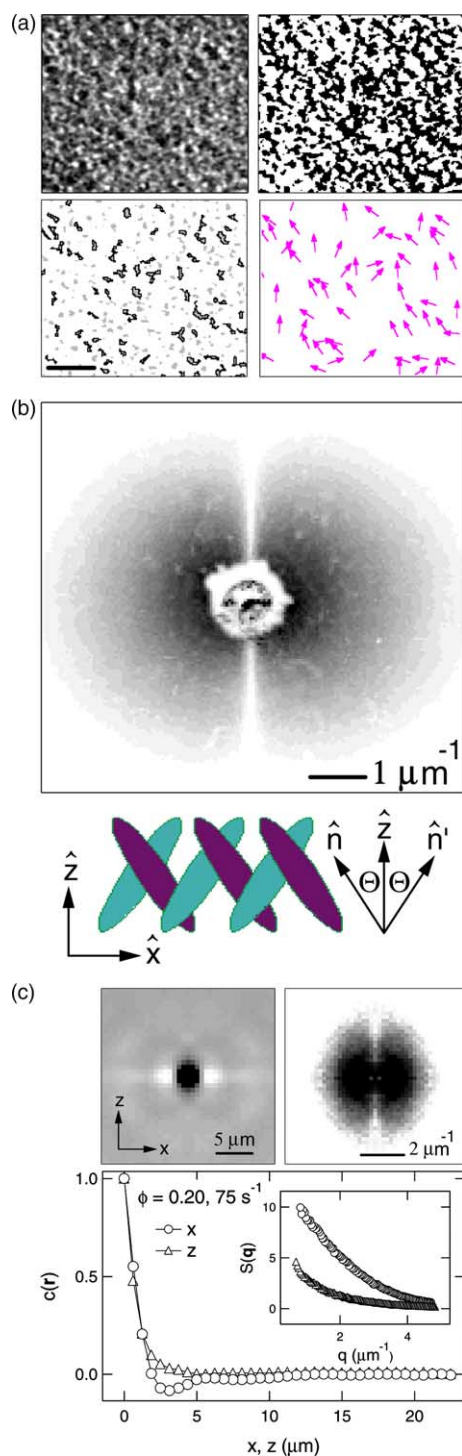
Fig. 7. (a) A typical micrograph for a sheared PI/PB blend, with the flow direction to the right and the vorticity direction from bottom to top. The real-space image (upper left) yields a binary image (upper right) of the distorted PI domains (black) in the continuous PB phase (white). Further thresholding preserves only the brightest regions (lower left, outlined in black, scale bar = 25 μm), where the orientation of the outlined shapes is used to extract the local field (lower right) that gives the orientation of domains. (b) Light-scattering pattern for the data in (a). The bottom panel shows a crude cartoon of the domain morphology, where the tilt angle Θ serves as a useful parameter for characterizing the shear response. The symmetry of this broadly tilted morphology with respect to the vorticity and flow directions can be inferred from the symmetry of the light-scattering patterns. (c) The upper left panel shows the two-point correlation function, $c(r)$, computed for the data in (a).

pattern. Projections of $c(\mathbf{r})$ along the flow and vorticity directions are shown in the pain panel of Fig. 7(c) and reveal the physical origin of this behavior. Weak correlation minima along the direction of flow indicate weak liquid-like order along that direction, which is what leads to the wing-like lobes of the scattering pattern. We have suggested that this type of weak anisotropic order arises from nearest-neighbor interactions of unstable HPI droplets, which appear to rock back and forth in the flow-vorticity plane, thus crowding out a region of excluded volume along the direction of flow [94], leading in turn to the minima in Fig. 7(c). With increasing HPI volume fraction, the two wings of the butterfly pattern retract along the flow direction and expand along the vorticity direction, suggesting that increased packing of such domains favors a larger component of orientation along the direction of flow [94]. We note that a domain pattern almost identical to that shown in Fig. 7 is also observed in sheared polymer–clay suspensions [96], where it is associated with flow-induced turbidity and the break up of a quiescent physical gel. It is also observed in a host of other sheared complex fluids that fall within the simple paradigm of soft interacting viscoelastic droplets suspended in a less viscous fluid [97], but its appearance in other systems that less clearly fall within this simple picture is intriguing and suggests a much wider relevance [98–100].

When the system is inverted, or when HPI forms the quiescent matrix or majority phase and LPB forms the quiescent droplet or dispersed phase, the shear response is completely different, reflecting the disparate rheology of the pure melt components. For $\phi_{\mathrm{HPI}} = 0.80$, a string-like pattern emerges at low shear rates, as shown in both real and reciprocal space in the upper panels of Fig. 8. It is important to note, however, that these strings are of a fundamentally different nature than those described in the previous paragraphs for low-molecular-weight polymer blends near a critical point of unmixing. Here, they form on purely hydrodynamic grounds because the droplet phase is of much lower viscosity than the continuous phase, and as such they are not associated with any softening in the interfacial tension [94]. At higher shear rates the response becomes more complicated. A 'walnut-like' pattern emerges, which is a superposition of a butterfly pattern and a vertical streak characteristic of strings. This pattern, shown with its real space structure in the middle panels of Fig. 8, looks like a superposition of the patterns observed from the LPB-rich-droplet and HPI-rich-droplet scenarios, which we suggest might be indicative of a shear-induced phase inversion in which the more viscous HPI matrix becomes the droplet phase [91,94]. A summary of the morphological evolution as a function of shear rate on each side of the phase inversion point is shown in the lower panel of Fig. 8.

4. Cessation of shear

In many applications, a blend will be brought suddenly from a strongly sheared state to a quiescent state, and the evolution of the domain morphology after such a 'shear quench' is both important and intriguing. As above, it depends on the proximity of the mixture to a critical point of unmixing as well as the

rheology of the pure melt components. Structural relaxation after cessation of shear also depends on the shear history of the mixture and the dominant mechanism of stress relaxation. The relaxation behavior of the well characterized PS/PB/DOP mixtures after a shear-quench has been studied extensively. Hashimoto and co-workers have investigated a quench from a shear rate above the critical threshold for mixing [82,101,102]. Immediately after cessation of shear, an isotropic scattering ring was observed. The peak position and intensity were found to be consistent with the intermediate to late stages of spinodal decomposition (SD) described in Section 2 of this paper. Takebe and Hashimoto also quenched the system to final shear rates within the nonequilibrium two-phase regime and observed an evolving spinodal ring superposed with an anisotropic relaxing domain structure.

In blends of low-vinyl polybutadiene and low-vinyl polyisoprene (LPB/LPI), relaxation after cessation of shear can be studied directly using optical microscopy. Fig. 9 shows typical micrographs of relaxation and coarsening after first reaching a steady state at different shear rates. Under such conditions, the kinetics can be quite complex. For example, after cessation of shear from string-like patterns in blends of polystyrene and polybutadiene (PS/PB) [103], low-vinyl polybutadiene and low-vinyl polyisoprene (LPB/LPI), and poly(dimethylsiloxane) and polyisobutylene [104–111], optical microscopy reveals the break-up of strings into necklace-like patterns, as shown in Fig. 10. The small bead-like domains retain a degree of alignment along the flow direction, reminiscent of a Raleigh instability [112]. The interplay of the relaxation of domain anisotropy with thermodynamic demixing is quite complex, however, particularly for the relaxation of string-like patterns that form near a critical point of unmixing, as shown in Fig. 11. The clear spinodal ring seen in the light scattering patterns demonstrates the evolution of the domains back to equilibrium (quiescent) coexisting compositions, highlighting the importance of thermodynamic mixing effects in relaxation after cessation of shear for this type of 'critical' system. In contrast, completely immiscible blends can likely be modeled exclusively using viscoelastic hydrodynamics without invoking any changes in domain composition upon cessation of flow. An example is shown in Fig. 12 for LPB/HPI blends at different compositions and shear rates. In a crude sense, the evolution of these patterns can be described as hydrodynamic coarsening driven by interfacial tension, although it takes a very long time for the initial droplet sizes to recover in these slow, concentrated viscoelastic blends. In all of these scenarios, the interplay of thermodynamics and viscoelaticity in multiphase polymer fluids under shear is of considerable importance, and yet this topic has received limited attention and remains poorly understood.

5. Conclusions

In conclusion, we have reviewed a number of experimental observations underlying the phenomenology of shear-induced structure in polymer blends, both immiscible and miscible.
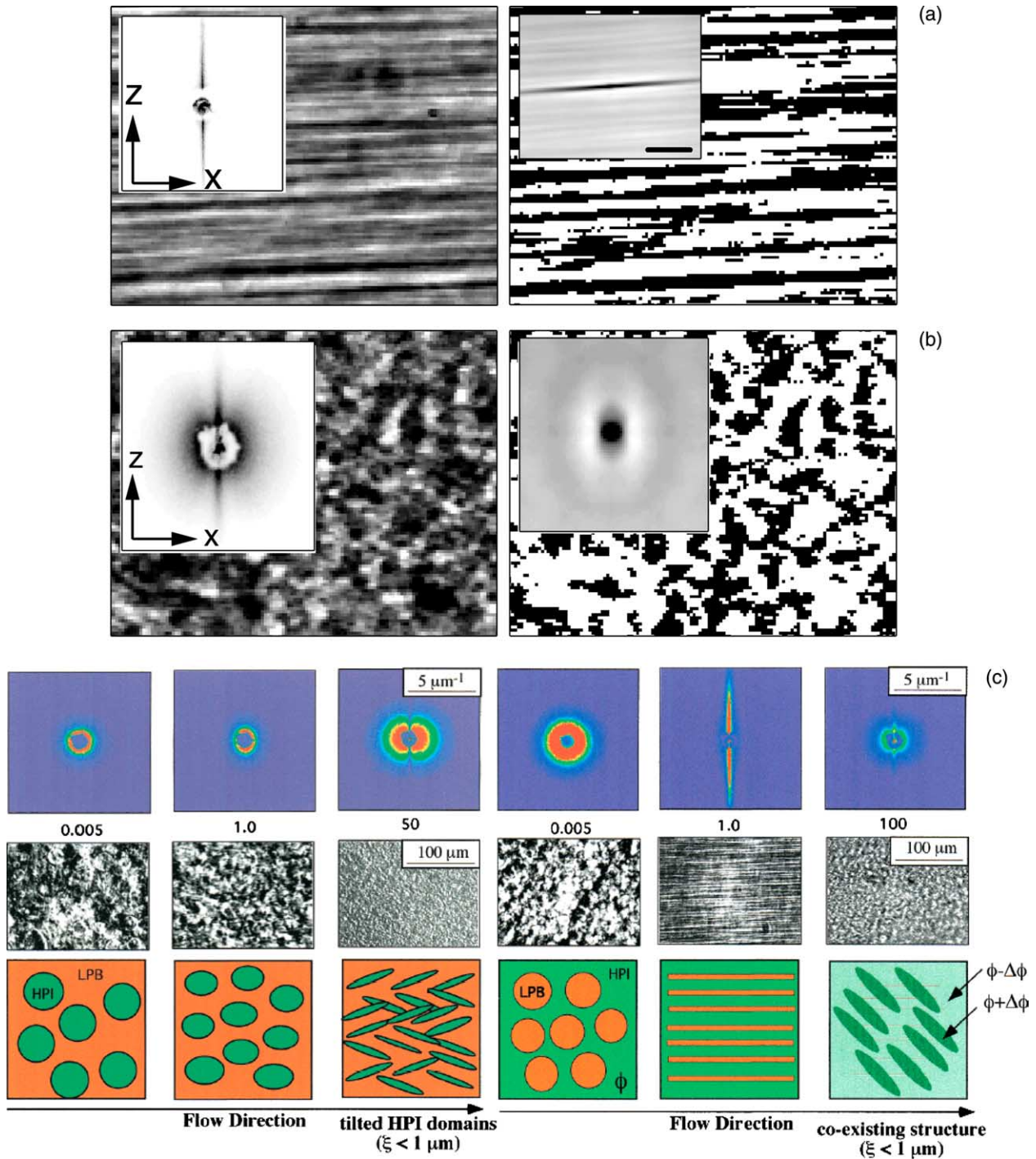
Fig. 8. (a) For $\phi=0.80$ at $\dot{\gamma}=10\ \mathrm{s}^{-1}$, the dispersed phase is PB, the matrix is PI, and the morphology is string-like. The string-like pattern is characterized by extended correlation along the flow direction and oscillatory order along the vorticity direction. This asymmetry is inverted in q-space, with reduced scattering along the flow direction and enhanced scattering along the vorticity direction. (b) At $\dot{\gamma}=100\ \mathrm{s}^{-1}$, the morphology of the $\phi=0.80$ sample has changed in a manner that suggests the presence of PI droplets dispersed in a PB matrix, as can be seen by comparing $c(r)$ with that obtained for $\phi=0.20$ in the limit of string shear. The light-scattering pattern is a superposition of a butterfly pattern and a vertical streak. (c) Small-angle light-scattering (SALS) patterns, phase-contrast optical micrographs, and domain morphology cartoons of the 20 volume ratio HPI (left) blend and 80 volume ratio HPI (right) blend at 130 °C at various shear rates, where the shear rate in inverse seconds is indicated under each light-scattering pattern. The flow direction is from left to right, and the vorticity direction is from top to bottom. Data were originally presented in Refs. [91,94].

When applicable, simple theoretical explanations have been used to interpret the measurements in a manner that emphasizes the underlying physics. The factors that influence non-equilibrium structure and phase behavior in sheared polymer blends and solutions are subtle, complex and varied, but a leading-order and unified (if perhaps somewhat over simplified) picture does emerge from the specific systems that we have considered here.
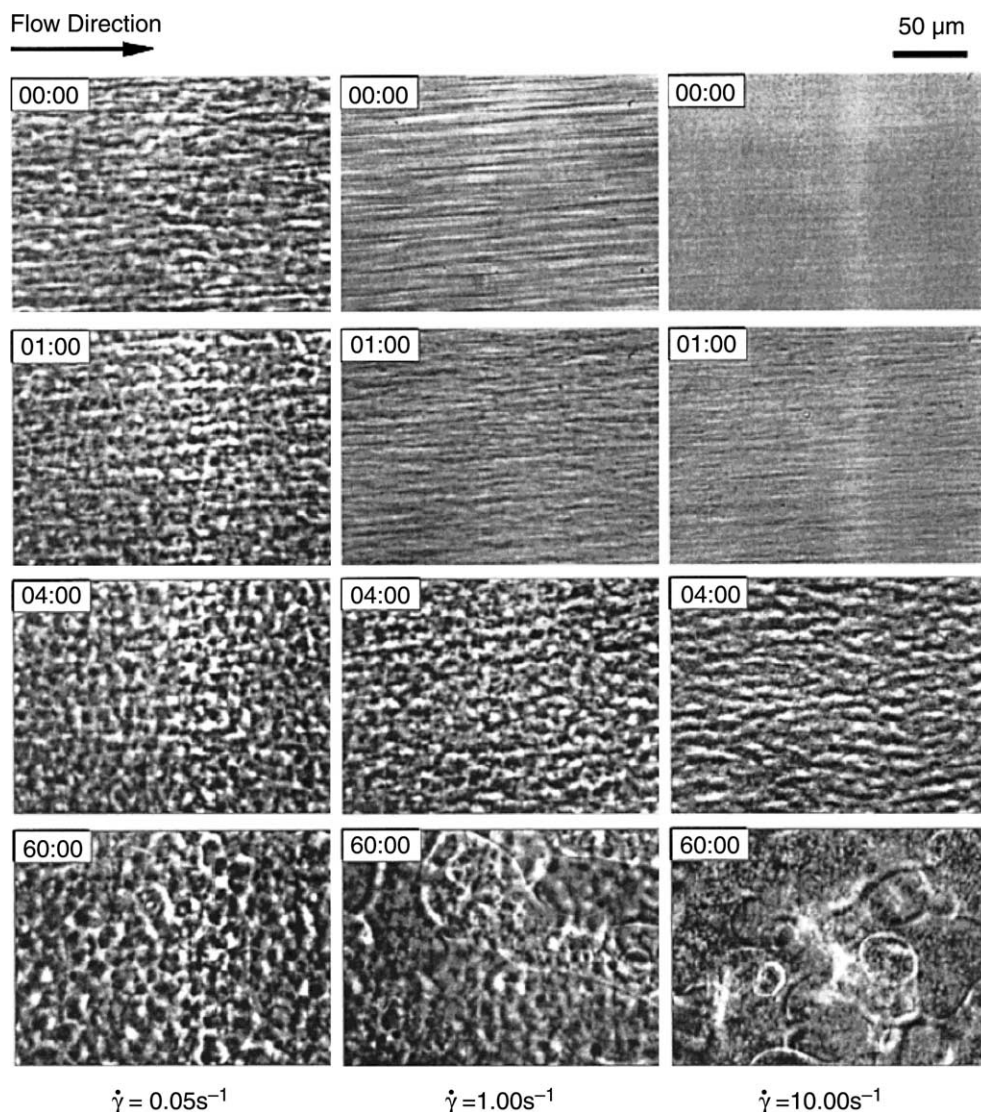
Fig. 9. Phase contrast optical micrographs of cessation-of-flow morphology obtained from LPB/LPI blend for different shear rates (labeled on the bottom) at a temperature of 110 °C with a LPI mass fraction of 0.43. PI-rich domains are evident as the darker areas. The original flow direction was horizontal. The time that has elapsed after the cessation of shear is indicated in each frame in minutes and seconds. Images were first published in Ref. [103].

For blends close to a thermodynamic critical point of unmixing, the dominant factor of influence is the softening of interfacial tension due to shear-induced mixing, which in turn leads to the formation of extended string-like patterns along the direction of flow. If such blends are driven further via a continuous increase in shear rate, one of two scenarios unfolds. Typically, if the components are reasonably Newtonian, the mixture eventually becomes homogeneous and miscibility is restored. This scenario is also played out in critical blends of Newtonian components with modest viscous asymmetry. If one of the miscible components is viscoelastic, however, the situation is more complex and less well understood. In some of the critical blends that we have studied, the mixing trend eventually ceases and the flow starts to have the opposite effect, manifest as a crossover from string-like patterns to butterfly patterns (Fig. 7). Such mixtures cannot usually be fully homogenized by shear, instead showing a mixing plateau like that in Fig. 6. The butterfly pattern, which can be viewed as

a consequence of rheological asymmetry, arises from the coupling between composition and elastic stress, and analogous patterns are associated with shear-induced turbidity in polymer solutions. Upon cessation of flow in these types of critical and near-critical mixtures, relaxation of anisotropy and structural coarsening as dictated by hydrodynamics are superposed on the return of the composition profile to equilibrium. An important scenario that has received limited consideration is that of two components having comparable viscoelasticity under shear near a critical point of unmixing, which is relevant to the flow processing of the commercially popular polyolefins.

For polymer blends that are completely immiscible—or in some sense infinitely far from a critical point of unmixing—there appears to be no significant shear-induced change in composition. No matter how strongly the fluid is sheared, a two-phase morphology of the pure melt components persists. In this case, the blend morphology is influenced solely by
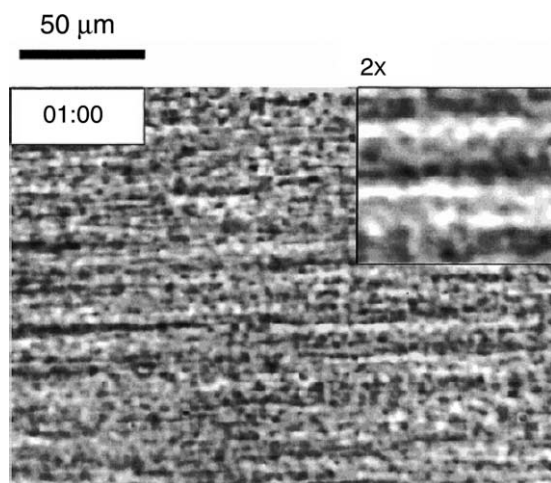
Fig. 10. Phase contrast micrograph of an LPB/LPI blend showing necklace-like domain structures 1 min after cessation of flow after steady-state shearing at 0.1 s^{-1}. The insert is enlarged by a factor of 2 for enhanced structural detail. These data originally appeared in Ref. [103].

rheology and hydrodynamics. When the more viscoelastic polymer is the continuous or 'matrix' phase, the morphology is string-like. When the more viscoelastic component is the dispersed or 'droplet' phase, the morphology is again that of the butterfly pattern (Fig. 7). Even when this type of asymmetric polymer blend is removed from a quiescent point of phase inversion—i.e. the composition where the quiescent 'matrix' phase becomes dispersed and the 'droplet' phase becomes continuous—the application of shear can induce a similar inversion in morphology. The rare scenario in which two immiscible viscoelastic components are rheologically similar has received limited attention. For fully immiscible Newtonian fluids of comparable viscosity, the sheared binary mixture typically forms a fine emulsion of modestly deformed monodisperse droplets. Upon cessation of shear, immiscible mixtures and blends relax and coarsen in a manner dictated by hydrodynamics in accordance with the rheology and volume fraction of the components.

As industrial applications for polymer blends and alloys increase—spreading out into the realm of biomaterials and biologically-based polymers—there will be new technological needs associated with the blending and compatiblization of polymers synthesized from newly created chemistries. Pure and applied research related to the shear-induced morphology and structural relaxation after cessation of shear in polymer blends will continue to become more and more important. While the phase behavior of binary polymer blends under quiescent conditions has been given significant theoretical and experimental attention, there is still a daunting and challenging task in developing a better understanding of the relationships between shear rate, rheology, phase behavior, and blend structure. Although the assumption of simple linear shear flow somewhat oversimplifies commercial blend processing, it does provide a much easier way to develop an understanding of more complicated flows involving multiphase materials, and it also provides insights that might lead to the opportunity for achieving better control of blend structure during processing, in
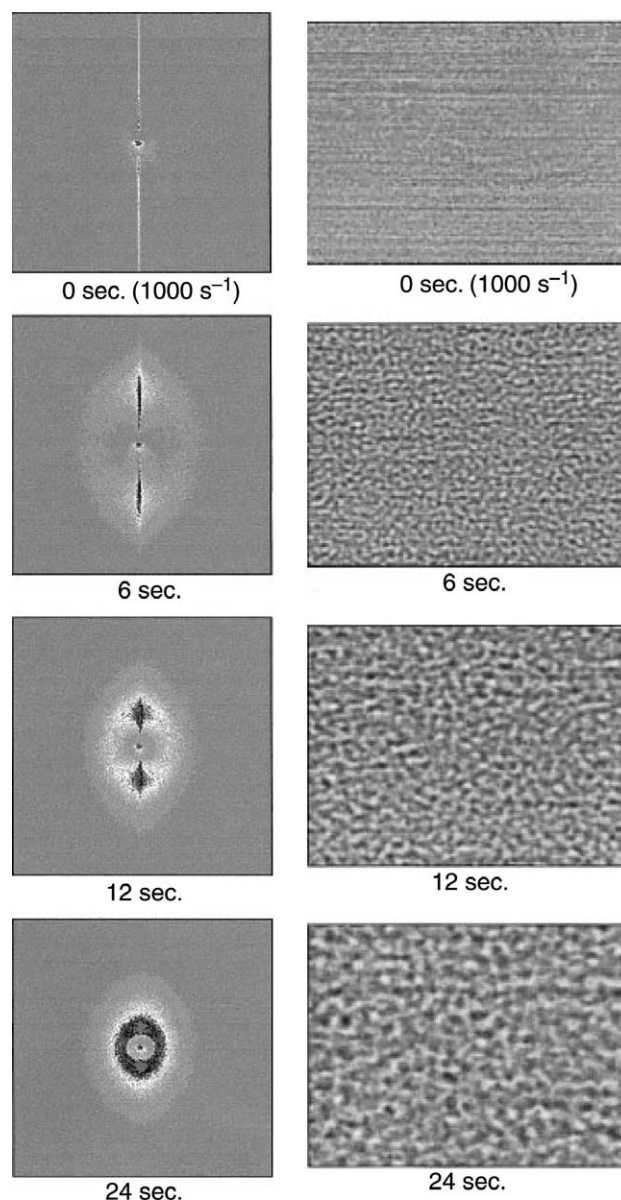
Fig. 11. Spinodal decomposition and stress relaxation in an unstable PS/PB mixture ($50/50$ $96.4 \times 10^3/22 \times 10^3$, 8% polymer in DOP, $T = 55$ °C, $T_s = 60$ °C) after cessation of shear. The times after shear quenching are shown in seconds. The mixture exhibits a string pattern at a shear rate of 1000 s^{-1}. After the flow is terminated, a spinodal ring is superimposed on an anisotropic scattering pattern that reflects the coarsening of anisotropic domains. Data were originally published in Ref. [31].

turn uncovering new routes to polymeric materials with novel and unique physical properties. The most evident shortcoming would seem to lie within the realm of theoretical and computational modeling, which we hope will be apparent from the review of the field that we have offered here. In particular, there is a great need to take the type of MCRG description appropriate for simple Newtonian mixtures near a critical point of unmixing and generalize these to fully viscoelastic components that can exhibit a significant degree of rheological asymmetry. Some efforts along this line have already been initiated [113–115], but there is still considerable room for further progress and achievement.
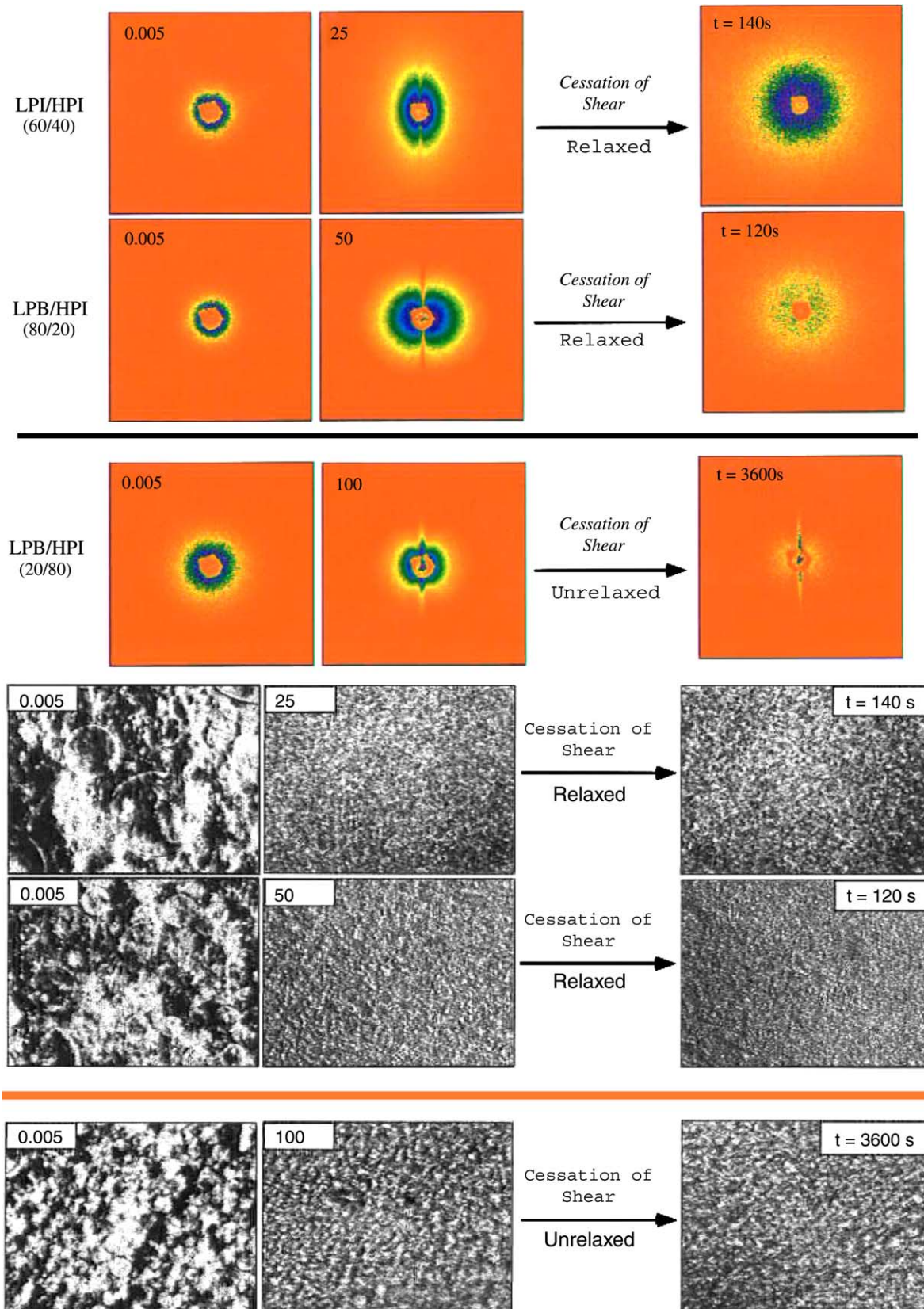
Fig. 12. Phase-contrast optical micrographs and small-angle light-scattering patterns after cessation of shear at 130 °C for three LPB/HPI blends with different HPI volume ratio: 0.40; 0.20; 0.80 (from top to bottom). The initial and final shear rates (in units of inverse seconds) are marked in the upper left corners. The width of each micrograph is 200 μm. The flow direction is from left to right, and the vorticity direction is from top to bottom. These results were originally published in Ref. [91].

Acknowledgements

References

[1] Hohenberg PC, Halperin BI. Rev Mod Phys 1977;49:435.

[2] Binder K. Phys Rev B 1977;15:4425.

[3] Kutner R, Binder K, Kehr KW. Phys Rev B 1982;26:2967.

[4] Kawasaki K. In: Domb C, Green MS, editors. Phase transitions and critical phenomena, vol. 5A. New York: Academic; 1976.

[5] Gunton JD, san Miguel M, Sahni PS. In: Domb C, Lebowitz JL, editors. Phase transitions and critical phenomena, vol. 9. London: Academic; 1983.

[6] Cahn JW. Trans Metal Soc AIME 1968;242:166.

[7] Hilliard JE. In: Anderson HL, editor. Phase transformations. Metals Park, OH: American Society for Metals; 1970.

[8] Cahn JW, Hilliard JE. J Chem Phys 1958;28:258.

[9] Cahn JW, Hilliard JE. J Chem Phys 1959;31:668.

[10] Cahn JW. J Chem Phys 1965;42:93.

[11] Cook HE. Acta Metall 1970;18:297.

[12] Beysens D, Gbadamassi M, Moncef-Bouanz B. Phys Rev A 1983;28: 2491.

[13] Beysens D, Gbadamassi M. Phys Rev A 1980;22:2250.

[14] Silberberg A, Kuhn W. Nature 1952;170:450.

[15] Silberberg A, Kuhn W. J Polym Sci 1954;13:21.

[16] Verstrate G, Phillipoff W. J Polym Sci, Polym Lett Ed 1974;12:267.

[17] Wu XL, Pine DJ, Dixon PK. Phys Rev Lett 1991;66:2408.

[18] Yanase H, Moldenaers P, Mewis J, Abetz V, Van Egmond J, Fuller GG. Rheol Acta 1991;30:89.

[19] Moses E, Kume T, Hashimoto T. Phys Rev Lett 1994;72:2037.

[20] Beysens D, Gbadamassi M, Boyer L. Phys Rev Lett 1979;43:1253.

[21] Onuki A, Kawasaki K. Ann Phys 1979;121:456.

[22] Menasveta MJ, Hoagland DA. Macromolecules 1991;24:3427.

[23] Migler K, Liu C-H, Pine DJ. Macromolecules 1996;29:1422.

[24] Kume T, Hattori T, Hashimoto T. Macromolecules 1997;30:427.

[25] Helfand E, Fredrickson GH. Phys Rev Lett 1989;62:2468.

[26] Milner ST. Phys Rev Lett 1991;66:1477.

[27] Rangel-Nafaile C, Metzner AB, Wissbrun KF. Macromolecules 1984; 17:1187.

[28] Tirrell M. Fluid Phase Equilib 1986;30:367.

[29] Hashimoto T, Takebe T, Suchiro S. J Chem Phys 1988;88:5874.

[30] Nakatani AI, Kim H, Takahashi Y, Matsushita Y, Takano A, Bauer B, et al. J Chem Phys 1990;93:795.

[31] Kim S, Hobbie EK, Yu J-W, Han CC. Macromolecules 1997;30: 8245.

[32] Hindawi IA, Higgins JS, Weiss RA. Polymer 1992;33:2522.

[33] Fernandez ML, Higgins JS, Richardson M. Polymer 1995;36:931.

[34] Gerard H, Higgins JS, Clarke N. Macromolecules 1999;32:5411.

[35] Chopra D, Vlassopoulos D, Hatzikiriakos SG. J Rheol 1998;42:1227.

[36] Martys NS, Douglas JF. Phys Rev E 2001;63:031205.

[37] Larson RG. Rheol Acta 1992;31:497.

[38] de la Cruz O. In: Araki T, Tran-Cong Q, Shibayama M, editors. Structure and properties of multiphase polymeric material. New York: Marcel Dekker; 1998 [chapter 1].

[39] Roe R-J, Rigby D. Adv Polym Sci 1987;82:105.

[40] Hashimoto T. Phase transition. London: Gordon and Breach; 1988 p. 47–119.

[41] Sung L, Nakatani AI, Han CC, Karim A, Douglas JF, Satija SK. Physica B 1997;241:1013.

[42] Sung L, Han CC. J Polym Sci, B: Polym Phys Ed 1995;33:205.

[43] Nakatani AI, Sung LP, Hobbie EK, Han CC. Phys Rev Lett 1997;79: 4693.

[44] Krishnan K, Almdal K, Burghardt WR, Lodge TP, Bates FS. Phys Rev Lett 2001;87:098301.

[45] Chu B. Laser light scattering: basic principles and practice. 2nd ed. San Diego, CA: Academic Press, Inc.; 1991.

[46] Higgins JS, Benoit HC. Polymers and neutron scattering. Oxford series on neutron scattering in condensed matter. New York: Oxford University Press; 1994.

[47] Søndergaard K, Lyngaae-Jørgensen J. Rheo-physics of multiphase polymeric systems—application of rheo-optical techniques in characterization. Lancaster, PA: Technomic Publishing; 1993.

[48] Fuller GG. Ann Rev Fluid Mech 1990;22:387.

[49] Janeschitz-Kriegl H. Polymer melt rheology and flow birefringence: polymers—properties and applications, vol. 6. Berlin: Springer; 1983.

[50] Nakatani AI. ACS Symp Ser 1995;597:1.

[51] Akcasu AZ, Bahar I, Erman B, Feng Y, Han CC. J Chem Phys 1992;97: 5782.

[52] Binder K. J Chem Phys 1983;79:6387.

[53] de Gennes PG. J Chem Phys 1980;72:4756.

[54] Pincus P. J Chem Phys 1981;75:1996.

[55] Han CC, Akcasu AZ. Ann Rev Phys Chem 1992;43:61.

[56] de Gennes PG. Scaling concepts in polymer physics. New York: Cornell University Press; 1979.

[57] Sanchez IC. Ann Rev Mater Sci 1983;13:387.

[58] Hammouda B, Benmouna M. J Polym Sci B 1995;33:2359.

[59] Taylor JK, Debenedetti PG, Graessley WW, Kumar SK. Macromolecules 1996;29:764.

[60] Binder K. J Chem Phys 1980;72:4756.

[61] Snyder HL, Meakin P. J Chem Phys 1983;79:5588.

[62] Siggia ED. Phys Rev A 1979;20:595.

[63] Motowoka M, Jinnai H, Hashimoto T, Qiu Y, Han CC. J Chem Phys 1993;99:2095.

[64] Schwahn D, Mortensen K, Yee-Madeira H. Phys Rev Lett 1987;58: 1544.

[65] Sato T, Han CC. J Chem Phys 1988;88:2057.

[66] Dudowicz J, Freed KF. Macromolecules 1991;24:5074.

[67] Dudowicz J, Freed MS, Freed KF. Macromolecules 1991;24:5096.

[68] Freed KF, Dudowicz J. Macromolecules 1996;29:625.

[69] Onuki A, Kawasaki K. Prog Theor Phys Suppl 1978;64:436.

[70] Onuki A, Yamazaki K, Kawasaki K. Ann Phys 1981;131:217.

[71] Onuki A. Physica A 1986;140:204.

[72] Hair DW, Hobbie EK, Nakatani AI, Han CC. J Chem Phys 1992;96: 9133.

[73] Hair DW, Hobbie EK, Douglas JF, Han CC. Phys Rev Lett 1992;68: 2476.

[74] Hobbie EK, Hair DW, Nakatani AI, Han CC. Phys Rev Lett 1992;69: 1951.

[75] Hobbie EK, Reed L, Huang CC, Han CC. Phys Rev E 1993;48:1579.

[76] Hobbie EK, Nakatani AI, Yajima H, Douglas JF, Han CC. Phys Rev E 1996;53:R4322.

[77] Hobbie EK, Nakatani AI, Han CC. Mod Phys Lett B 1994;8:1143.

[78] Stepanek P, Lodge TP, Kedrowski C, Bates FS. J Chem Phys 1991;94: 8289.

[79] Takebe T, Sawaoka R, Hashimoto T. J Chem Phys 1989;91:4369.

[80] Takebe T, Fujioka K, Sawaoka R, Hashimoto T. J Chem Phys 1990;93: 5271.

[81] Fukjioka K, Takebe T, Hashimoto T. J Chem Phys 1993;98:717.

[82] Hashimoto T, Takebe T, Asakawa K. Physica A 1993;194:338.

[83] (a) Taylor GI. Proc R Soc A 1932;138:41.
    (b) Taylor GI. Proc R Soc A 1934;146:501.

[84] Onuki A. Phys Rev A 1986;34:R3528.

[85] Onuki A. Int J Thermophys 1989;10:293.

[86] Onuki A. Phys Rev A 1987;35:5149.

[87] Hobbie EK, Kim S, Han CC. Phys Rev E 1996;54:R5909.

[88] Moldover MR. Phys Rev A 1985;31:1022.

[89] Yonghua Yao. Unpublished results.

[90] Yu J-W, Douglas JF, Hobbie EK, Kim S, Han CC. Phys Rev Lett 1997; 78:2664.

[91] Jeon HS, Nakatani AI, Hobbie EK, Han CC. Langmuir 2001;17: 3087.

[92] (a) Jeon HS, Hobbie EK. Phys Rev E 2001;63:061403. (b) also see erratum Jeon HS, Hobbie EK. Phys Rev E 2001;64:049901.
[93] Jeon HS, Shou Z, Chakrabarti A, Hobbie EK. Phys Rev E 2002;65: 041508.
[94] Hobbie EK, Jeon HS, Wang H, Kim H, Stout DJ, Han CC. J Chem Phys 2002;117:6350.
[95] Hobbie EK, Migler KB. Phys Rev Lett 1999;82:5393.
[96] Lin-Gibson S, Schmidt G, Kim H, Han CC, Hobbie K. J Chem Phys 2003;119:8080.
[97] Hobbie EK, Lin-Gibson S, Wang H, Pathak JA, Kim H. Phys Rev E 2004;69:061503.
[98] Hoekstra H, Mewis J, Narayanan T, Vermant J. Langmuir 2005;21: 11017.
[99] Vermant J, Solomon MJ. J Phys Condens Matt 2005;17:R187.
[100] Vermant J. Curr Opin Colloid Interface Sci 2001;6:489.
[101] Takebe T, Hashimoto T. Polym Commun 1988;29:227.
[102] Takebe T, Hashimoto T. Polym Commun 1988;29:261.
[103] Kielhorn L, Colby RH, Han CC. Macromolecules 2000;33:2486.
[104] Vinckier I, Mewis J, Moldenaers P. Rheol Acta 1999;38:65.
[105] Vinckier VI, Mewis J, Moldenaers P. Rheol Acta 1999;38:198.
[106] Minale M, Moldenaers P, Mewis J. J Rheol 1999;43:815.
[107] Yang H, Zhang H-J, Moldenaers P, Mewis J. Polymer 1998;39:5731.
[108] Mewis J, Yang H, Van Puyvelde P, Moldenaers P, Walker LM. Chem Eng Sci 1998;53:2231.
[109] Van Puyvelde P, Yang H, Moldenaers P, Mewis J. J Colloid Interface Sci 1998;200:86.
[110] Vinckier I, Mewis J, Moldenaers P. J Rheol 1997;41:705.
[111] Vinckier I, Mewis J, Moldenaers P. Rheol Acta 1997;36:513.
[112] Tomotika S. Proc R Soc London Ser A 1935;150:322.
[113] Zhang Z, Zhang H, Yang Y. J Chem Phys 2001;115:7783.
[114] Tanaka H. J Chem Phys 1994;100:5323.
[115] Tanaka HM. Prog Theor Phys 1998;100:1281.
[116] Han CC, Yao Y. China patent Application 200510123609.9.
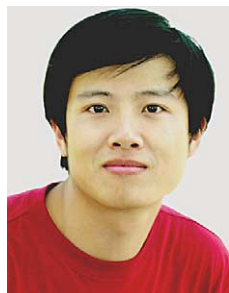
Yonghua Yao is currently a graduate student at the State Key Laboratory of Polymer Physics and Chemistry, Joint Laboratory of Polymer Science and Materials, Institute of Chemistry, Chinese Academy of Sciences. He received his bachelor's degree in chemical engineering at Beijing Forestry University in 2000, where he was award for his thesis titled 'Enhancement of petrolic production efficiency' under the Prof. Jingyi An of Technical Institute of Physics and Chemistry, Chinese Academy of Sciences. Later he joined Prof. Charles C. Han's group for his master's and PhD degrees, where he investigated phase separation and crystallization of polymer blends and solutions with and without shear field.
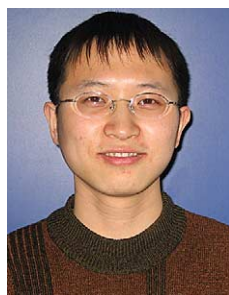
Ruoyu Zhang was born on November 1982, and obtained his bachelor's degree in 2003 in Beijing Institute of Technology. His was majored in polymer engineering and science for his BS degree, and then entered into Prof. Han's group to study polymer physics as his major. Now he is a Doctor candidate at the Institute of Chemistry Chinese Academy Sciences. One of his research subjects is polymer blends under simple shear using a small angle light scattering with in situ microscopy to study the dynamic mixing process.

Charles C. Han received his BS degree in Chemical Engineering from the National Taiwan University in 1966. He received his master's degree in Physical Chemistry from the University of Houston in 1969, and his PhD degree in Physical Chemistry from the University of Wisconsin, Madison in 1973. He joined the National Bureau of Standards (changed to National Institute of Standards and Technology) in 1974. He was a research scientist, then group leader for the polymer blends group and later the multiphase materials group. He was elected as the NIST fellow in 1995. He joined the Institute of Chemistry, the Chinese Academy of Sciences in 2002 as the chief scientist and the director for the joint laboratory of polymer science and materials. His research interests include light scattering, dynamic light scattering, small angle neutron scattering and small angle X-ray scattering in polymer research, order–disorder transition and pattern formation of block copolymers, equilibrium phase behavior and kinetics of spinodal decomposition of polymer mixtures and crystallization behaviors, shear dependence of the static and kinetic phase behavior of polymer mixtures and its application in polymer processing, and more recently on the in-reactor alloying of polyolefins with compound catalyst. He has won many awards and prizes, including the Dillon Medal of American Physical Society, Humboldt Senior Research Award from Alexander von Humboldt Foundation, and the High Polymer Physics Prize, American Physical Society. He has published more than 300 research papers, and co-authored or co-edited 15 books. He also have 14 US and Chinese patents which have been approved or disclosed.

Erik Hobbie is a senior research scientist in the Polymers Division at the National Institute of Standards and Technology (NIST) in Gaithersburg, Maryland. He received his doctorate from the University of Minnesota in 1990 and then came to NIST as a National Research Council Postdoctoral Fellow. His research covers a broad range of topics in rheology, materials science and soft condensed matter physics, including liquid crystals, polymer blends and solutions, nanocomposites, colloids and emulsions.